Journal of
Mechanics of Materials and Structures

SWITCHING DEFORMATION MODES IN POST-LOCALIZATION SOLUTIONS WITH A QUASIBRITTLE MATERIAL

Pierre Bésuelle, René Chambon and Frédéric Collin

Volume 1, Nº 7 *September 2006*

mathematical sciences publishers

JOURNAL OF MECHANICS OF MATERIALS AND STRUCTURES
Vol. 1, No. 7, 2006

SWITCHING DEFORMATION MODES IN POST-LOCALIZATION SOLUTIONS WITH A QUASIBRITTLE MATERIAL

PIERRE BÉSUELLE, RENÉ CHAMBON AND FRÉDÉRIC COLLIN

Localization in a quasibrittle material is studied using a local second-gradient model. Since localization takes place in a medium assumed to be initially homogeneous, nonuniqueness of the solutions of an initial boundary value problem is then also studied. Using enhanced models generalizes the classical localization analysis. In particular, it is necessary to study solutions more continuous (that is, continuous up to the degree one) than the ones used in analysis involving classical constitutive equations. Within the assumptions done, it appears that localization is possible in the second-gradient model if it is possible in the underlying classical model. Then the study of nonuniqueness is conducted for the numerical problem, using different first guesses in the full Newton–Raphson procedure solving the incremental nonlinear equations. Thanks to this method, we are able to simulate qualitatively the nonreproducibility of usual experiment in the postpeak regime.

1. Introduction

Modeling the degradation of materials is a very challenging task. If the degradation is sufficiently high — if the material exhibits some softening (here in a vague sense) — it is now well known that some unpleasant features appear both in experiments and in computations.

From the experimental point of view, as soon as the softening is reached, it seems that the behavior is poorly reproducible or nonreproducible. The first reason is that in main cases strain localization occurs which means that contrary to current assumptions, laboratory samples are not strained homogeneously up to the failure. Moreover localization patterns themselves are not easily reproduced. Let us first quote Desrues and Viggiani [2004], who performed some biaxial tests twice:

> [E]very test is somewhat unique as for the patterns of strain localization (location of the shear band, appearance of nonpersistent and/or multiple bands).

Quite clearly such behavior is related to the loss of uniqueness of the problem (that is, in the reported case the biaxial test) which allows shear bands to emerge. But, what is clear in [Desrues and Viggiani 2004] is that there is a large variability in the observed patterns. This means that there is not only one alternative solution involving a unique localized band. If it is quite clear that if orientation and width of the bands are easily reproduced, on the contrary the number of bands and their position as well as their persistence cannot be predicted in advance. This has some consequences for the load versus displacement curves which can exhibit very different results in their postpeak parts (that is, when some localization can be

Keywords: continuum with microstructure, second gradient, finite element, bifurcation, strain localization, mode switching, reproducibility.

P.B. gratefully acknowledges financial support for a two-month stay for at the University of Liège through a Research Fellowship of the Fonds National de la Recherche Scientifique (FNRS) of Belgium.

expected). This is clearly illustrated in [Desrues and Hammad 1985] or in [Desrues 1984] where the two curves of duplicate tests are in many cases rather different as soon as the peak value is attained. Other similar observations about tests performed twice can be found in [Viggiani et al. 2001]. These results are often interpreted as the consequence of some (unfortunately unknown) initial imperfection in the studied samples, and based on the deterministic principle, it is argued that if the initial state is completely known the problem should disappear.

Following the previous ideas, numerical modeling of such postpeak phenomena is usually achieved by introducing some (deterministic) initial imperfection into the computation, and it is believed that uniqueness of the solution is restored. Consequently changing the imperfection can change the final solution of the computation since it is assumed that there is a correspondence between a given imperfection and the resulting solution. Unfortunately we demonstrated recently that this way of thinking may be erroneous; see [Chambon and Moullet 2004]. For the same imperfection several (properly converged) solutions can be found provided an appropriate searching algorithm is used. Recently, introducing an initial fluctuation of the mechanical properties has been used to deal with this problem, for instance in [Nübel and Huang 2004]. In the quoted paper the introduction of this initial fluctuation is achieved by initializing randomly the density for a model sensitive with respect to this parameter. The computations performed seem very similar to what is usually observed. However, even in this case, it seems that the author assumes implicitly that uniqueness is restored. Alternative solutions should be searched in order to clarify this point.

Another way is followed in the numerical experiments detailed in the present paper. We choose to solve the "perfect" (which means without any intentional imperfection) problem, and we try to exhibit several solutions for this problem. Usually the method used to find alternative solutions is related to a spectral analysis of the linearized velocity problem. Numerically this is achieved by searching when the least eigenvalue of the tangent stiffness matrix related to the velocity discretized problem goes to zero; see for instance [de Borst 1986] or [Ikeda and Murota 2002]. This method is based on a linearization of the problem which is completely sound if the nonlinear problem is incrementally linear. Since we use an elastoplastic model, elastic up to a given threshold and exhibiting a sudden softening as soon as this threshold is reached, there are many possible linearizations depending on the choice of the unloading area within the computed domain. Then the drawback of such a method is that the mode corresponding to the null eigenvalue which allows theoretically to follow the bifurcated solution can correspond for some point of the studied structure to a constitutive branch (loading or unloading) different to the one used to compute the linearized stiffness matrix. In this paper we prefer to follow the ideas initially applied in [Chambon et al. 2001b] where the solution for a time step is searched with a Newton–Raphson method with different first estimations which can (if the problem has more than one solution) yield different properly converged solutions.

On the other hand, it is now well known that localizations cannot be properly modeled with classical media since this implies rupture without energy consumption as proved by Pijaudier-Cabot and Bažant [1987]. Enhanced models are necessary. However, contrary to what is often believed, the use of an enhanced model does not guarantee uniqueness of the solution of the corresponding boundary value problems; this has been demonstrated in [Chambon et al. 1998; Chambon and Moullet 2004], the latter employing the same model used in this paper. But it seems that the result is more general. Challamel and Hijaj [2005] also found solutions for the same problem, but using a nonlocal, enhanced model.

In this paper a second-gradient theory is used in conjunction with the method to search alternative solutions recalled above. The first section of this paper is devoted to a brief recall of the model used and of the principle of its numerical implementation.

In order to be able to perform easily different computations, the element has been first implemented in the general purpose finite element code Lagamine developed at University of Liège [Charlier 1987], and we checked the accuracy of this implementation using extended tests. This is described in the second section of this paper.

Then a localization analysis is performed in the third section of the paper. Such an analysis is necessarily different from the original ones of [Rudnicki and Rice 1975] since the type of discontinuity assumed in the aforementioned reference cannot be used due to the second-order terms.

After briefly recalling the method, the fourth section deals with the numerical experiments of nonuniqueness and describes computations exhibiting switching modes. Such mode switching has already been studied by Ikeda et al. [1997] in a different context. It has been made mainly for the incrementally linear comparison solid, which on the one hand allows a sound mathematic treatment, but on the other discards modes involving a change in the loading branches of the constitutive equations. Here, as explained above, no assumption is done concerning the behavior but only a numerical treatment of the problem is made.

As for our notations, a component of a tensor (or vector) is denoted by the name of the tensor (or vector) accompanied by the indices. All tensorial indices are in lower position, since there is no need to distinguish between covariant and contravariant components. Upper indices have specific meanings defined in the text. The summation convention with respect to repeated tensorial indices is used.

2. Local second-gradient models

2.1. ***A microstructured continuum with kinematic constrains.*** Models with microstructure descend from the pioneer works of the Cosserat brothers [Cosserat and Cosserat 1909], via [Toupin 1962], [Mindlin 1964] and [Germain 1973]. They use an enriched kinematic description of the continuum, with respect to classical continua, recalled hereafter. In addition to the displacement field, u_i, a second-order tensor, the microkinematic gradient v_{ij}, is introduced. Particular subclasses of enriched models introduce a constraint on the microkinematic field. For example, Cosserat models can be viewed as a microstructured model for which the microstrain is vanishing, that is, the symmetric part of the tensor v_{ij} is zero. In the same spirit, (local) second-gradient models assume that the microkinetic gradient is equal to the displacement gradient $v_{ij} = \partial u_i/\partial x_j$, where x_j is the spatial coordinate. Recently, such models have been developed for geomaterials [Chambon et al. 2001a; Matsushima et al. 2002; Chambon and Moullet 2004] and for metals [Fleck and Hutchinson 1997].

For local second-gradient models, the virtual work principle can be summarized as follows. For every kinematically admissible virtual displacement fields $u_i^\star$,

$$\int_\Omega \left(\sigma_{ij}\varepsilon_{ij}^\star + \Sigma_{ijk}\frac{\partial^2 u_i^\star}{\partial x_j\,\partial x_k} \right) dv = \int_\Omega G_i u_i^\star\, dv + \int_{\partial\Omega} \left(t_i u_i^\star + T_{ij}\frac{\partial u_i^\star}{\partial x_j} \right) ds, \tag{1}$$

where σ_{ij} is the Cauchy stress, $\varepsilon_{ij}^\star$ is the virtual macrostrain, Σ_{ijk} is the dual static variable associated to the second gradient of the virtual displacement, the so-called *double stress*; see [Germain 1973]. Further,

G_i is the body force per unit volume, t_i is the traction force per unit surface and T_{ij} is the double force per unit surface. However t_i and T_{ij} cannot be taken independently, since $u_i^\star$ and $\partial u_i^\star/\partial x_j$ are not independent. More conveniently, the virtual work of external forces can be rewritten using the normal derivative $Du_i = n_k\,\partial u_i/\partial x_k$ on the boundary. Here and in the following n_k is the normal to the boundary (assumed to be regular).

$$\int_\Omega \left(\sigma_{ij}\varepsilon_{ij}^\star + \Sigma_{ijk}\frac{\partial^2 u_i^\star}{\partial x_j\,\partial x_k}\right) dv = \int_\Omega G_i u_i^\star\, dv + \int_{\partial\Omega}\left(p_i u_i^\star + P_i Du_i^\star\right) ds, \tag{2}$$

where p_i and P_i are two independent variables which can be prescribed on the boundary.

For such a class of models, the balance equations and boundary conditions yield

$$\frac{\partial\sigma_{ij}}{\partial x_j} - \frac{\partial^2\Sigma_{ijk}}{\partial x_j\,\partial x_k} + G_i = 0, \tag{3}$$

$$\sigma_{ij}n_j - n_k n_j D\Sigma_{ijk} - \frac{D\Sigma_{ijk}}{Dx_k}n_j - \frac{D\Sigma_{ijk}}{Dx_j}n_k + \frac{Dn_l}{Dx_l}\Sigma_{ijk}n_j n_k - \frac{Dn_j}{Dx_k}\Sigma_{ijk} = p_i, \tag{4}$$

$$\Sigma_{ijk}n_j n_k = P_i, \tag{5}$$

where Dq/Dx_j denotes the tangential derivatives of any quantity q:

$$\frac{Dq}{Dx_j} = \frac{\partial q}{\partial x_j} - n_j Dq. \tag{6}$$

2.2. ***Numerical implementation in a finite element code.*** A direct application of virtual work principle (2) to solve equations of a boundary value problem needs to use C^1 elements. To avoid this constraint, a weak form of equation (2) can be introduced with help of a Lagrange multipliers field λ_{ij}, which yields, for any time t and any kinematically admissible virtual fields $u_i^\star$ and $v_{ij}^\star$,

$$\int_{\Omega^t}\left(\sigma_{ij}^t\frac{\partial u_i^\star}{\partial x_j^t} + \Sigma_{ijk}^t\frac{\partial v_{ij}^\star}{\partial x_k^t} + \lambda_{ij}^t\left(\frac{\partial u_i^\star}{\partial x_j^t} - v_{ij}^\star\right)\right) dv = \int_{\Omega^t} G_i^t u_i^\star dv + \int_{\partial\Omega^t}\left(p_i^t u_i^\star + P_i Du_i^\star\right) ds, \tag{7}$$

and for any virtual field $\lambda_{ij}^\star$,

$$\int_{\Omega^t}\lambda_{ij}^\star\left(\frac{\partial u_i^t}{\partial x_i^t} - v_{ij}^t\right) dv = 0. \tag{8}$$

A complete description of the numerical treatment can be found in [Chambon and Moullet 2004]. The problem is discretized in time and for each finite step a full Newton–Raphson is applied to solve the resulting nonlinear problem. In order to get the equations suitable for Newton–Raphson technique, the unbalanced quantities are computed after the n-th iteration of the current time step. The same equations are applied for the $n+1$-th iteration, assuming these equations are well balanced. Then, by differentiation, one gets a proper linearization of the set of equations for the Newton–Raphson method. Equations are written in the actual configuration and the small strain assumption is not made, which introduces some geometrical terms in the linearized equations.

The finite element is organized with 8 nodes for the displacement field u_i, 4 nodes for the displacement gradient field v_{ij}, and a single node for the Lagrange multipliers field λ_{ij}. The element was introduced

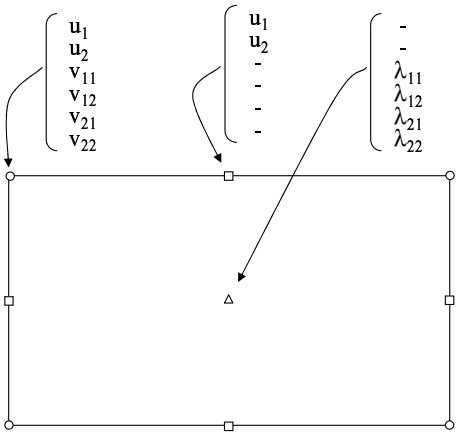

Figure 1. Nodal variables used in the finite element introduced in Lagamine.

in the finite element code Lagamine, initially developed at Liège University in Belgium [Charlier 1987]. The element used in Lagamine to implement our second-gradient model contains in fact 9 nodes each with 6 possible degrees of freedom. For the present application, some of these are not used (see Figure 1): only 36 degrees of freedom are activated by element [Bésuelle 2005].

The following algorithm is adopted for computing one time step from $t-\Delta t$ to t.

(1) Initial configuration: stress $\sigma^{t-\Delta t}$, double stress $\Sigma^{t-\Delta t}$, coordinates $x^{t-\Delta t}$.

(2) Assumption on the final configuration for the first iteration $n = 1$:
- initialization of the increment of nodal values $[\Delta U^{t,n}_{\text{node}}]$,
- update coordinates: $x^{t,n}$.

(3) Beginning of the iteration n.

(4) For each element:
- for each integration point:
  - compute the strain rate, the rotation rate and the second-gradient rate,
  - compute $\Delta\sigma^{t,n}$ and $\Delta\Sigma^{t,n}$ using the constitutive equations,
  - update the stress and the double stress $\sigma^{t,n} = \sigma^{t-\Delta t} + \Delta\sigma^{t,n}$, $\Sigma^{t,n} = \Sigma^{t-\Delta t} + \Delta\Sigma^{t,n}$,
  - compute the consistent tangent stiffness matrices of constitutive laws.
- compute the element stiffness matrix.
- compute the element out of balance forces.

(5) Compute the global stiffness matrix.

(6) Compute the global out of balance forces.

(7) Compute the corrections $[\delta U^{t,n}_{\text{node}}]$ of the increment of nodal values by solving the Newton–Raphson linearized system.

(8) Check the accuracy of the computed solution:
- if convergence: go to 9,

- if no convergence: update the new assumed final configuration, $n = n + 1$ and go to 3.

(9) End of the step.

3. Validation

3.1. ***Constitutive model: a quasibrittle material.*** The constitutive model used in this paper is the same as in [Matsushima et al. 2002] and [Chambon and Moullet 2004], and it can be decoupled into two independent relations. The first is classical, and links the stress to the displacement gradient; it is a Von Mises elastoplastic law based on the Prandt–Reuss model, with a strain softening regime. The second relation gives the double stress as a function of the gradient of the field v_{ij} (that is, the second gradient of the displacement); it is a linear elastic law. Concerning the constitutive equation used here, we emphasize that the classical part of the model involves no hardening but only sudden softening as soon as a threshold is attained. Moreover this part is not a hyperelastoplastic model, contrary to the ones used for bifurcation analyses in [Steinmann et al. 1997; Borja 2002; Ikeda et al. 2003]. From a thermodynamical point of view it would presumably be better to use the hyperelastoplastic model, but in the second-gradient context it is then necessary to build up a new theory. This has already been done in [Tamagnini et al. 2001b] and [Chambon et al. 2004], but the implementation of such a model in a finite element code has not yet been made.

The classical relation is

$$\dot{\sigma} = 3\,K\,\dot{e},$$

$$\overset{\triangledown}{s}_{ij} = \begin{cases} 2\,G_1\,\dot{\varepsilon}_{ij} & \text{for } \|\varepsilon\| \le e_{\lim}, \\ 2\,G_1\left(\dot{\varepsilon}_{ij} - \dfrac{G_1 - G_2}{G_1}\,\dfrac{s_{kl}\dot{\varepsilon}_{kl}}{\|s\|^2}s_{ij}\right) & \text{for } \|\varepsilon\| > e_{\lim}, \end{cases} \tag{9}$$

where $\overset{\triangledown}{s}_{ij}$ is the Jaumann rate of the deviatoric Cauchy stress tensor, $\dot{\varepsilon}_{ij}$ is the deviatoric strain rates, $\dot{\sigma}$ is the mean stress rate and $\dot{e}$ is the mean strain rate. K, G_1 and G_2 are the bulk modulus, the shear moduli before peak and after peak, respectively. $\|\varepsilon\|$ is the second invariant of the Green–Lagrange deformation tensor, $e_{\lim}$ is a deformation parameter of the model which corresponds to the deviatoric stress peak.

The bulk modulus K is assumed to be constant. The elastic shear modulus available for unloading is assumed to be constant, while an exponential function is assumed as follows for the shear modulus after the yield point so that the material could reach its residual state smoothly:

$$G_2 = \bar{G}_2 \exp\left(\frac{\bar{G}_2}{G_1 e_{\lim} - \sigma_{\text{res}}}(\|\varepsilon\| - e_{\lim})\right), \tag{10}$$

where $\bar{G}_2$ is the value of the shear modulus just after yielding and σ_{res} is the residual deviatoric stress.

The second-gradient law has been chosen as simple as possible. It is a particular case of the more general isotropic linear relation derived in [Mindlin 1964], involving six parameters corresponding to five independent coefficients. The following relation is slightly different from the one in [Matsushima

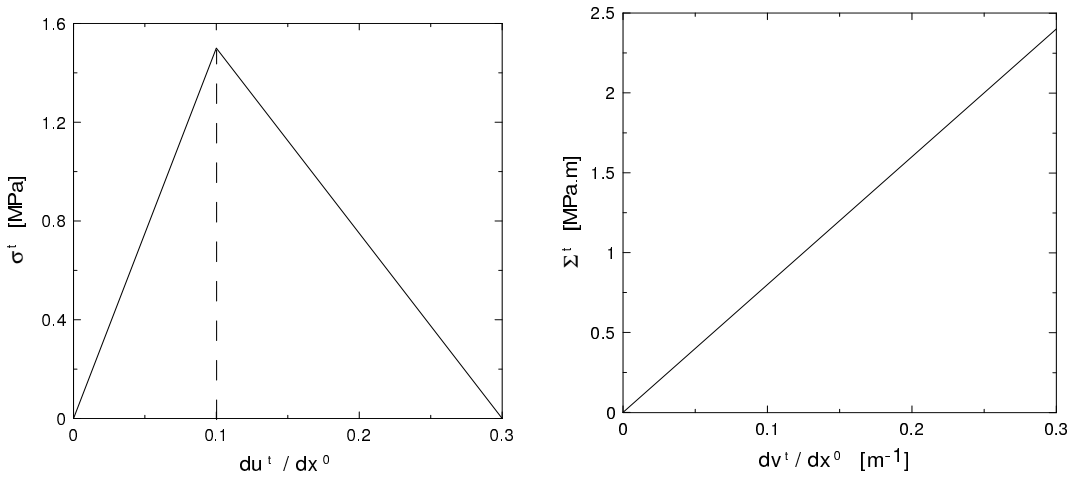

Figure 2. Constitutive relations in the one-dimensional case: (left) first grade term; (right) second grade term.

et al. 2002] and [Chambon and Moullet 2004], in that some inaccuracies have been corrected:

$$\begin{bmatrix} \overset{\triangledown}{\Sigma}_{111} \\ \overset{\triangledown}{\Sigma}_{112} \\ \overset{\triangledown}{\Sigma}_{121} \\ \overset{\triangledown}{\Sigma}_{122} \\ \overset{\triangledown}{\Sigma}_{211} \\ \overset{\triangledown}{\Sigma}_{212} \\ \overset{\triangledown}{\Sigma}_{221} \\ \overset{\triangledown}{\Sigma}_{222} \end{bmatrix} = \begin{bmatrix} D & 0 & 0 & 0 & 0 & D/2 & D/2 & 0 \\ 0 & D/2 & D/2 & 0 & -D/2 & 0 & 0 & D/2 \\ 0 & D/2 & D/2 & 0 & -D/2 & 0 & 0 & D/2 \\ 0 & 0 & 0 & D & 0 & -D/2 & -D/2 & 0 \\ 0 & -D/2 & -D/2 & 0 & D & 0 & 0 & 0 \\ D/2 & 0 & 0 & -D/2 & 0 & D/2 & D/2 & 0 \\ D/2 & 0 & 0 & -D/2 & 0 & D/2 & D/2 & 0 \\ 0 & D/2 & D/2 & 0 & 0 & 0 & 0 & D \end{bmatrix} \begin{bmatrix} \partial \dot{v}_{11}/\partial x_1 \\ \partial \dot{v}_{11}/\partial x_2 \\ \partial \dot{v}_{12}/\partial x_1 \\ \partial \dot{v}_{12}/\partial x_2 \\ \partial \dot{v}_{21}/\partial x_1 \\ \partial \dot{v}_{21}/\partial x_2 \\ \partial \dot{v}_{22}/\partial x_1 \\ \partial \dot{v}_{22}/\partial x_2 \end{bmatrix}, \tag{11}$$

where $\dot{v}_{ij}$ is the material time derivative of v_{ij}, and $\overset{\triangledown}{\Sigma}_{ijk}$ is the Jaumann double stress derivative, defined by $\overset{\triangledown}{\Sigma}_{ijk} = \dot{\Sigma}_{ijk} + \Sigma_{ljk}\omega_{li} + \Sigma_{imk}\omega_{mj} + \Sigma_{ijp}\omega_{pk}$, where ω_{li} is the spin tensor.

3.2. ***One-dimensional simulation.*** In order to validate the implementation of the element in Lagamine, first a one-dimensional compression is computed. This problem has analytic solutions under the assumption of small strain; see [Chambon et al. 1998]. The bar is 1 meter long. The degrees of freedom u_1, v_{11}, v_{12} and v_{21} are blocked at each node, the direction 2 being the direction of compression. In order to study the symmetrical localized solution composed of a central patch in the softening loading part and two end patches in the elastic unloading part, two elements at the middle of the bar have a e_{lim}-value reduced by 2%. The constitutive parameters are the same as those used in [Matsushima et al. 2002]:

$$\begin{gathered} G_1 = 16.875\,\text{MPa}, \quad \bar{G}_2 = 0\,\text{MPa}, \quad e_{\text{lim}} = 0.082, \\ K = -7.5\,\text{MPa}, \quad D = 0.08\,\text{MN}. \end{gathered} \tag{12}$$

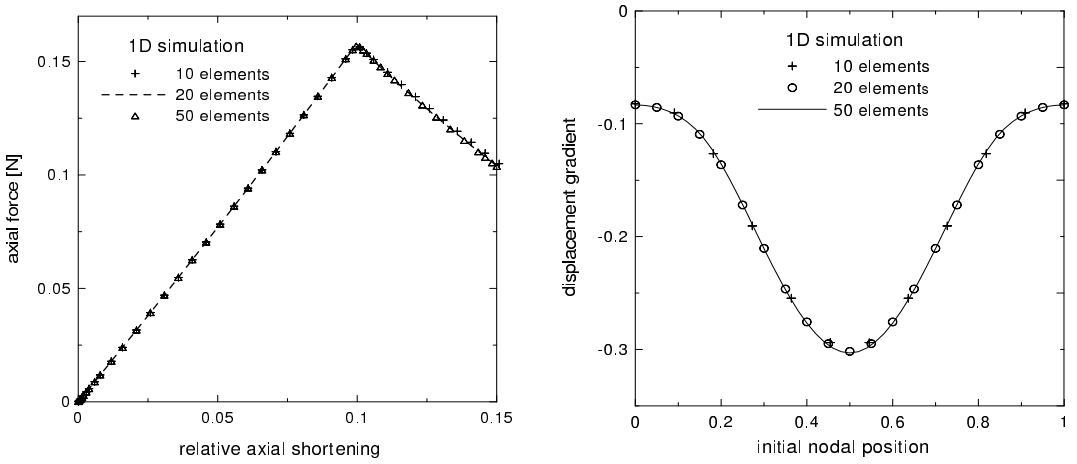

Figure 3. Comparison of three mesh refinements in one-dimensional simulations: (left) evolution of the resulting force versus the axial shortening, and (right) displacement gradient along the bar.

The two constitutive relations are plotted in Figure 2. To observe the influence of the mesh on the numerical solutions, three mesh refinements are used, with 11, 20 and 50 elements, respectively. The three solutions are very close (Figure 3), in terms of force versus bar shortening and deformation profile.

3.3. ***Two-dimensional simulation.*** A biaxial test is computed in this section as an example of a two-dimensional problem. Figure 4 shows the initial configuration of the specimen. It is 0.5 m wide and 1 m high (and 1 m thick). The (classical) surface tractions per unit area at both sides of the specimen are set equal to zero. The external additional double forces per unit area P_i are assumed to be zero all along the boundaries. At the top there is a smooth rigid plate remaining horizontal. Through this plate

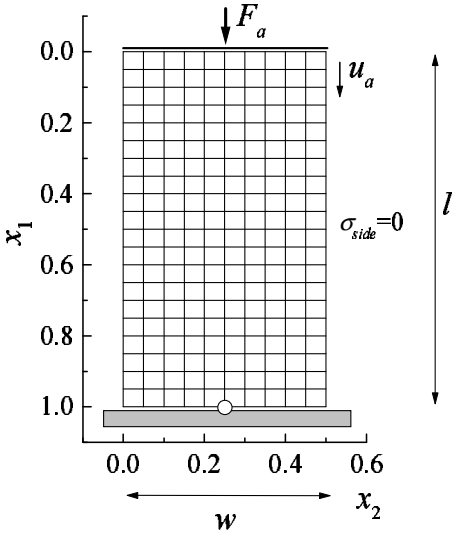

Figure 4. Initial configuration and boundary condition for biaxial test.

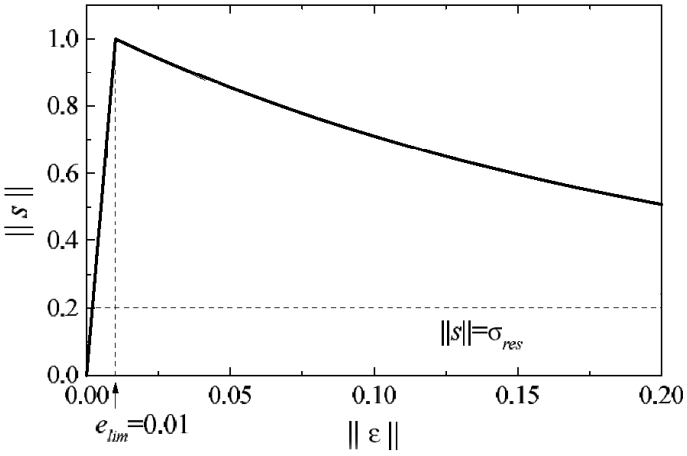

Figure 5. Classical part of the constitutive relation.

a compressive force F_a is applied. The vertical displacement of this top plate is denoted by u_a. At the bottom, there is another rigid and smooth plate, which remains horizontal too. The central point of the bottom plate is fixed to avoid rigid body displacement. The classical part of the constitutive relation is plotted in Figure 5. The parameters are chosen as follows:

$$G_1 = 50\,\text{MPa}, \quad \bar{G}_2 = -2\,\text{MPa}, \quad e_{\text{lim}} = 0.01,$$
$$K = 97.3856\,\text{MPa}, \quad \sigma_{\text{res}} = 0.2\,\text{MPa}, \quad D = 0.2\,\text{kN}. \tag{13}$$

Several meshes are compared: structured meshes with 10×20, 15×30, 20×40 and 40×80 elements, and an unstructured mesh with 300 elements. The left bottom element of the mesh has a e_{lim}-value reduced of 10% in order to force a localization band in this area. Here, we try to find similar solutions; that is, we don't try to find more than one alternative solution contrary to what is done in the following sections.

The implementation of our element in a general purpose code allows us to go further in the validation procedure. For example, we can work with unstructured meshes, an impossibility until now. Moreover, the use of a general code makes it possible to compare more precisely the similarities (and likely the differences) between different computations. It is often especially difficult to compare solutions of the same problem obtained with different meshes. In the following computations, in order to determine the width of the shear band, instead of comparing contours of some variable (often obtained by some interpolation procedure), we have chosen to look directly at the part of the computed body which loads plastically (inside the localized band). For this purpose, we have marked by a small open square the (plastically) loading Gauss points. In the area where there are no such marks the material unloads elastically.

The localization patterns of solutions (Figure 6) are very close, and the band thickness depends very little on the mesh size. We want here to emphasize a new result: an unstructured mesh changes neither the orientation nor the width of the band even if its position seems to be a little shifted. However, we have to keep in mind that, since we use an imperfection related to an element, the problems solved in

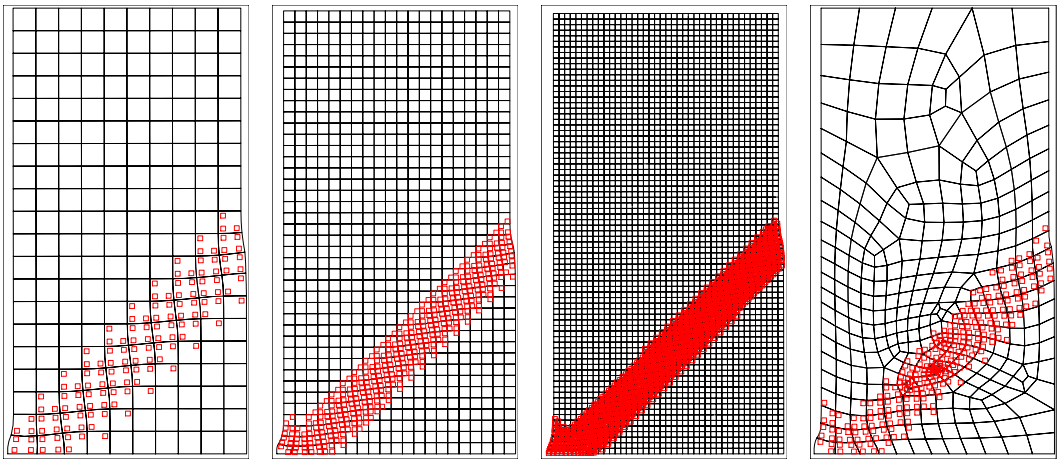

Figure 6. Comparison of the localization patterns for the four meshes 10×20, 20×40, 40×80 and an unstructured mesh with 300 elements, respectively. The imperfection is located in the left bottom element. The squares correspond to the integration points which are in the softening loading part; the other integration points are in the elastic regime.

the four cases are not exactly the same. The curves of the loading force versus the specimen shortening (Figure 7) are also very close. The step of band propagation from the imperfection concerns the force peak zone, and as soon as the band is completely propagated through the specimen, the force decreases. When the number of elements is sufficiently high (about 300 elements), or, more objectively, when there are at least about three elements in the band thickness, the curves are perfectly superimposed.

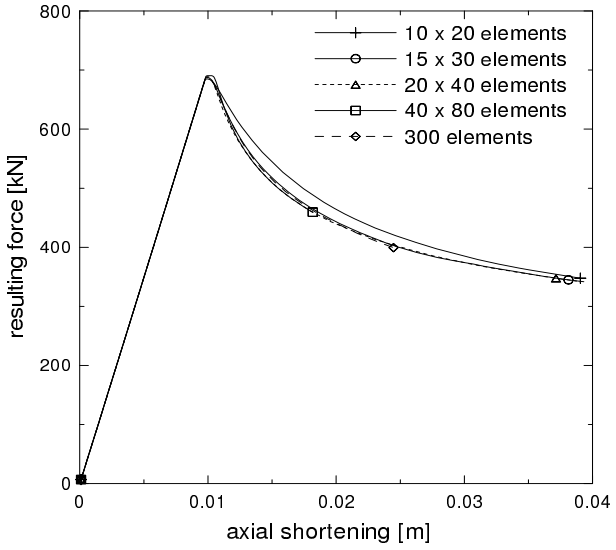

Figure 7. Comparison of the resulting force versus axial shortening curves for the same meshes.

4. Nonuniqueness of solutions

The aim of this section is to show that as soon as strain localization is possible, there can exist several solutions to a boundary value problem, despite of the use of a second-gradient model. Moreover, consistent with experimental observations, it is possible that the computed solutions switch from one pattern to another.

Generalizing Hill's uniqueness theorem [Hill 1958], Chambon and Moullet [2004] demonstrated that, under certain assumptions on the model, local second-gradient models (in the small strain framework) enjoy a uniqueness property. These results, applied to the biaxial problem, allow us to prove that uniqueness of solution is preserved in the elastic regime. In the biaxial problem described above, this unique solution is the homogeneous elastic response for which the response of the second-gradient model is similar to the response of a classical law. When the state of stress reaches the peak of the law, the uniqueness theorem cannot be applied, and, consistent with the numerical results in [Chambon et al. 1998] and in [Chambon and Moullet 2004], more than one solution is possible. It is then interesting to try to generalize the shear band analysis in the spirit of [Rudnicki and Rice 1975].

We present here a bifurcation analysis to search the condition for existence of a localized band. Applied to the second-gradient model used here, such an analysis is a generalization of the pioneering work of Rice [1976] and Rudnicki and Rice [1975]. We will show that for second-gradient models, at least when classical and second-gradient parts are decoupled, the bifurcation analysis is reduced to a bifurcation analysis on the classical part of the constitutive relation. However, the result is weaker in the sense that as soon as the criterion is met, localized solutions are possible, but not in all cases. Let us emphasize this point. This means that the second-gradient model and the underlying classical model have the same prebifurcation curve since second-gradient effects are only active for inhomogeneous fields. But the bifurcation point of the second-gradient model is located beyond the bifurcation point of the classical model, with the difference depending on the size of the modeled sample. It is likely that from the limit case of an infinite sample, both models have the same bifurcation point. Clearly the postbifurcation behavior is different for the two models.

The classical part of the rate law is assumed to be bilinear, and the second gradient law linear. We restrict this analysis by assuming that the so-called small strain assumption holds. So we use the ordinary material stress rates instead of some objective ones like the Jaumann stress rates:

$$\dot{\sigma}_{ij} = K^e_{ijkl}\,\frac{\partial \dot{u}_k}{\partial x_l} \quad \text{or} \quad \dot{\sigma}_{ij} = K^{ep}_{ijkl}\,\frac{\partial \dot{u}_k}{\partial x_l} \quad \text{depending on} \quad \frac{\partial \dot{u}_k}{\partial x_l},$$

$$\dot{\Sigma}_{ijk} = A_{ijklmn}\,\frac{\partial^2 \dot{u}_l}{\partial x_m\,\partial x_n}.$$

The nonhomogeneous solution is assumed to have the form of a planar band with unit normal n_i. Inside and outside the band, the velocity gradient depends only on the position across the band. The velocity gradient inside and outside the band must have the form

$$\frac{\partial \dot{u}^\zeta_i}{\partial x_j} = \frac{\partial \dot{U}_i}{\partial x_j} + g^\zeta_i\, n_j,$$

where $\zeta = 1$ inside the band, and $\zeta = 0$ outside. The displacement gradient $\partial \dot{U}_i / \partial x_j$ is assumed homogeneous, and $g_i^\zeta = g_i^\zeta(\alpha)$ are arbitrary vectors depending on the position $\alpha = x_k\, n_k$ across the band. g_i^1 characterizes the strain field inside the band and g_i^0 corresponds to the near field on each side of the band. To insure the strain continuity, we assume that

$$g_i^1 = g_i^0 \tag{14}$$

at the boundaries of the band. This point deserves a discussion. This is a salient difference with the localization analysis for classical materials. To some extent, we use a second-gradient theory in order to have more regular solutions. From the theoretical point of view, solutions have to be C^1 continuous. Moreover, contrary to what happens for a classical model, a discontinuity of the strain rate could imply that some forces are infinite. Consequently a classical shear band analysis cannot apply a priori to the models used here.

The C^1 continuity requirement is not imposed in the localization analysis developed in [Huang et al. 2005; Iordache and Willam 1998]. In this case, a discontinuity of the Cosserat rotation rate is assumed, which should imply an infinite curvature. However, these studies used *pure* Cosserat models, which means that there is no link between microrotation and macrorotation (see for instance [Chambon et al. 2001a] for a study of the difference between the pure Cosserat model and second-gradient Cosserat model). An analysis allowing discontinuities might be interesting, but an analysis with C^1 continuous fields should be made as well, as we suggested in [Chambon et al. 2001a]. Our opinion is corroborated by the results of Iordache and Willam [1998]. These authors found that the analysis with discontinuities gives results corresponding to compaction or extension bands—for the case for which Cosserat effects are vanishing, which means finally for a classical model.

For simplicity's sake, we assume that the direction of g_i^ζ over the band is constant and then

$$g_i^\zeta(\alpha) = g^\zeta(\alpha)\, m_i^\zeta,$$

where $g^\zeta(\alpha)$ are scalar functions and m_i^ζ are constant unit vectors. To simplify the notation, we consider that the solutions on each side of the band are the same (symmetry with respect to the band) and we do not make any difference between the solution on one side and that on the other.

In each point of the body, the stress and double stress fields satisfy conditions of equilibrium in (3). Because the prebifurcation field is presumed uniform, the stress rate and double stress rate at the onset of localization satisfy

$$\frac{\partial \dot{\sigma}_{ij}^\zeta}{\partial x_j} - \frac{\partial^2 \dot{\Sigma}_{ijk}^\zeta}{\partial x_j\, \partial x_k} = 0. \tag{15}$$

Moreover, at the boundaries of the band, conditions (4) and (5) must be satisfied (the tangential derivative on the boundaries of the band are zero because the displacement gradient depends only on α):

$$\dot{\sigma}_{ij}^0 n_j - \frac{\partial \dot{\Sigma}_{ijk}^0}{\partial x_p} n_p n_j n_k = \dot{\sigma}_{ij}^1 n_j - \frac{\partial \dot{\Sigma}_{ijk}^1}{\partial x_p} n_p n_j n_k, \tag{16}$$

$$\dot{\Sigma}_{ijk}^0 n_j n_k = \dot{\Sigma}_{ijk}^1 n_j n_k, \tag{17}$$

where $(\cdot)^0$ and $(\cdot)^1$ denote quantities outside and inside the band, respectively.

The equilibrium condition inside and outside the band can be written

$$K^{\zeta}_{ijkl}\, n_j n_l\, (g^{\zeta}_k)' - A_{ijklmn}\, n_j n_k n_m n_n\, (g^{\zeta}_l)''' = 0, \tag{18}$$

where $(g^{\zeta}_k)'$ is the derivative of $g^{\zeta}_k(\alpha)$ in the direction orthogonal to the band. It seems reasonable to assume that $K^1_{ijkl} = K^{ep}_{ijkl}$ and $K^0_{ijkl} = K^e_{ijkl}$.

The limit conditions at the two boundaries of the band depend on the constitutive relation which is considered on each side of the interface. For classical constitutive laws, it can be shown that the softer response (that is, the one corresponding to the tensor $\mathbf{K}^{ep}$) can be considered on each side of the interface to track the first bifurcation condition (see [Bésuelle and Rudnicki 2004] for a review).

Here, Equation (17) becomes:

$$A_{ijklmn}\, n_j n_k n_m n_n\, \left((g^0_l)' - (g^1_l)'\right) = 0. \tag{19}$$

Since function $g_i(\alpha)$ is continuous at the boundaries of the band (see Equation (14)) and since the material is loading inside the band and unloading outside, this means that it undergoes a neutral loading:

$$K^{ep}_{ijkl}\, \frac{\partial \dot{u}^0_k}{\partial x_l}\bigg|_{\alpha=\alpha_a \text{ or } \alpha_b} = K^{e}_{ijkl}\, \frac{\partial \dot{u}^0_k}{\partial x_l}\bigg|_{\alpha=\alpha_a \text{ or } \alpha_b}. \tag{20}$$

Then the limit condition (16) can be written

$$K^{ep}_{ijkl}\, n_j n_l\, \left(g^0_k - g^1_k\right) - A_{ijklmn}\, n_j n_k n_m n_n\, \left((g^0_l)'' - (g^1_l)''\right) = 0. \tag{21}$$

Finally the problem can be summarized as follows:

- outside the band, the following condition, which comes from Equation (15), must be satisfied:

$$\mathcal{K}^e_{ij}\, (g^0_j)' - \mathcal{A}_{ij}\, (g^0_j)''' = 0; \tag{22}$$

- inside the band, once more coming from Equation (15), we observe that

$$\mathcal{K}^{ep}_{ij}\, (g^1_j)' - \mathcal{A}_{ij}\, (g^1_j)''' = 0; \tag{23}$$

- there must exist two values α^a and α^b for which the following conditions are satisfied:

$$\mathcal{A}_{ij}\, \left((g^0_j)' - (g^1_j)'\right) = 0, \tag{24}$$

  which comes from Equation (19), and

$$\mathcal{A}_{ij}\, \left((g^0_j)'' - (g^1_j)''\right) = 0, \tag{25}$$

  which comes from Equation (21),

where $\mathcal{K}^{ep}_{ik} = K^{ep}_{ijkl}\, n_j n_l$, $\mathcal{K}^e_{ik} = K^e_{ijkl}\, n_j n_l$ and $\mathcal{A}_{il} = A_{ijklmn}\, n_j n_k n_m n_n$. Note that $|\alpha^a - \alpha^b|$ corresponds to the band thickness.

Since Equations (22)–(23) are ordinary linear differential equations, one can search solutions of the form $g^{\zeta}_i(\alpha) = \gamma_\zeta\ \exp(\lambda_\zeta \alpha)\, m^{\zeta}_i$, where γ_ζ are nonzero constants (if $\gamma_\zeta = 0$, there is no localization) and λ_ζ are the two unknowns of the problem. Then one has to solve

$$(\mathcal{K}^{ep}_{ij} - (\lambda_1)^2 \mathcal{A}_{ij})\, m^1_j = 0 \tag{26}$$

and

$$(\mathcal{K}^e_{ij} - (\lambda_0)^2 \mathcal{A}_{ij})\, m^0_j = 0. \tag{27}$$

There is then a solution corresponding to a nonuniform field if

$$\det(\mathcal{K}^{ep}_{ij} - \Lambda_1\, \mathcal{A}_{ij}) = 0, \tag{28}$$

and

$$\det(\mathcal{K}^e_{ij} - \Lambda_0\, \mathcal{A}_{ij}) = 0, \tag{29}$$

where $\Lambda_\zeta = (\lambda_\zeta)^2$.

A localized solution corresponds to a strain field involving an extremum. Then this implies $\Lambda_1 < 0$ for an harmonic form for $g^1(\alpha)$ inside the band (while one expects $\Lambda_0 > 0$ outside the band for a hyperbolic form). In fact, we are also guided in this reasoning by the one dimensional analytical solutions obtained by Chambon et al. [1998] and by El Hassan [1997], who demonstrated that the hyperbolic form corresponds to a kind of boundary layer.

Equation (28) is an algebraic equation of degree 3. The third-order term reads $\det(\mathcal{A})$ whereas the zero-order terms reads $\det(\mathcal{K}^{ep})$. If Λ_a, Λ_b, Λ_c are the solutions of this equation, then consequently

$$\det(\mathcal{A})\Lambda_a\ \Lambda_b\ \Lambda_c = \det(\mathcal{K}^{ep}). \tag{30}$$

As a consequence of the choice of an isotropic tensor for the second-order part of the model, we have $\mathcal{A} = D\,\mathbf{I}$, where $\mathbf{I}$ is the identity tensor. This can be easily checked for the particular value of A_{ijklmn} detailed in Equation (11). So, $\det(\mathcal{A}) = D^3$.

Before the onset of localization, the roots are expected to be positive (no localized solutions). So without any additional assumption, the bifurcation condition as in classical (bilinear) constitutive equation [Chambon et al. 2000] is

$$\det(\mathcal{K}^{\mathbf{ep}}) \le 0. \tag{31}$$

If we assumed the incremental continuity of the classical part of the law, then a necessary and sufficient condition for the sign of one root to change (that is, to have a vanishing root) is

$$\det(\mathcal{K}^{\mathbf{ep}}) = 0, \tag{32}$$

which corresponds to the classical bifurcation condition for a classical bilinear law. In this case the result can be found directly by inspecting the annulment of the zero-order term of Equation (28). Moreover, $\det(\mathcal{K}^{\mathbf{e}}) > 0$, and so the solution g^0_i outside the band is hyperbolic.

As far as the band thickness is concerned, it is given by finding α_a and α_b that satisfy the double condition (24)–(25), which can be reduced here to

$$\big((g^1)' - (g^0)'\big)\big|_{\alpha=\alpha_a \text{ or } \alpha_b} = 0 \quad \text{and} \quad \big((g^1)'' - (g^0)''\big)\big|_{\alpha=\alpha_a \text{ or } \alpha_b} = 0.$$

Note that we assume in the particular form (11) that the parameter D is constant and positive. With other models such as the ones detailed in [Chambon et al. 2001a], plasticity can also occur in the second-gradient part of the model and in this case, D can evolves during the loading. Since the order of magnitude of the thickness of the band is given by the inverse of λ_ζ, the evolution of the thickness of the band is related to the variations of D and of $\det(\mathcal{K}^{\mathbf{ep}})$ according to Equation (30).

Coming back to the model defined by Equation (11), where D is assumed to be constant, the thickness of the emerging band corresponding to condition (32) is infinite and decreases when $\det(\mathcal{K}^{\mathbf{ep}})$ decreases. Since an infinite thickness for a finite size boundary value problem is not realistic, the onset of localization can be somewhat delayed when second-gradient models are used. Consequently this criterion is not completely similar to the one of classical media. It is a necessary condition of localization, however since second-gradient models implicitly include an internal length, it is possible that this criterion could be met but without loss of uniqueness for some "small" (with respect to the internal length) problems.

For the particular law adopted in Equations (9)–(11), the bifurcation criterion is satisfied after the deviatoric stress peak.

5. Switching mode of deformation

5.1. ***Algorithm for nonuniqueness search.*** When several solutions for a given boundary value problem exist, it can be difficult to know that they exist and to find the other (or some of the other) solutions, especially when the boundary value problem is nonlinear.

As we recall from Section 1, it is not satisfactory to search the null space of one eigenvalue of the tangent stiffness matrix related to the linearized discretized velocity problem. This way is useful for incrementally linear problems such as the ones induced by using a large strain elastic theory, but is only a guess for incrementally nonlinear problems arising when a constitutive equation incorporates some unloading branches.

For numerical computations involving classical constitutive equations, we have developed an algorithm to search several (eventual) solutions to a problem. It takes advantage of the fact that at the beginning of a time step, for the first iteration, the nodal quantities denoted $[\Delta U^{t_n}_{\text{node}}]$ in the algorithm presented in Section 2.2 can be freely chosen. The standard choice is to use nodal values related to the ones obtained at the end of the previous time step. Such a choice applied to an initially homogeneous problem generally (though not in all cases) leads to the homogeneous solution. If a random initialization is adopted for $[\Delta U^{t_n}_{\text{node}}]$, then it is possible to find nonhomogeneous solutions. In fact, for classical continua, our experience (see [Chambon et al. 2001b]) is that as soon as uniqueness is lost, the duplication of numerical experiments can yield different solutions, changing only some numerical parameters such as the time step size or the first guess of a given time step. Since all of them are properly converged, this means that they are all different solutions of the same initial boundary value problem defined by the same history of boundary conditions.

Recently, this algorithm has been adapted to second-gradient models [Chambon and Moullet 2004]. It has also been implemented in Lagamine, leading to the following numerical results.

5.2. ***Numerical loss of uniqueness.*** We present in Figure 8 several localized solutions (well converged) found after a few random initializations. The random initialization algorithm has been activated after a specimen shortening of 0.012 m while the stress peak corresponds to a shortening of 0.01 m. In order to clearly visualize the localized zones, the (plastically) loading Gauss points are marked with small open squares. As in experiments, the width of the bands is completely reproducible. On the contrary, the position, the number, and, more generally, the patterning between several bands are quite different from one numerical experiment to another.

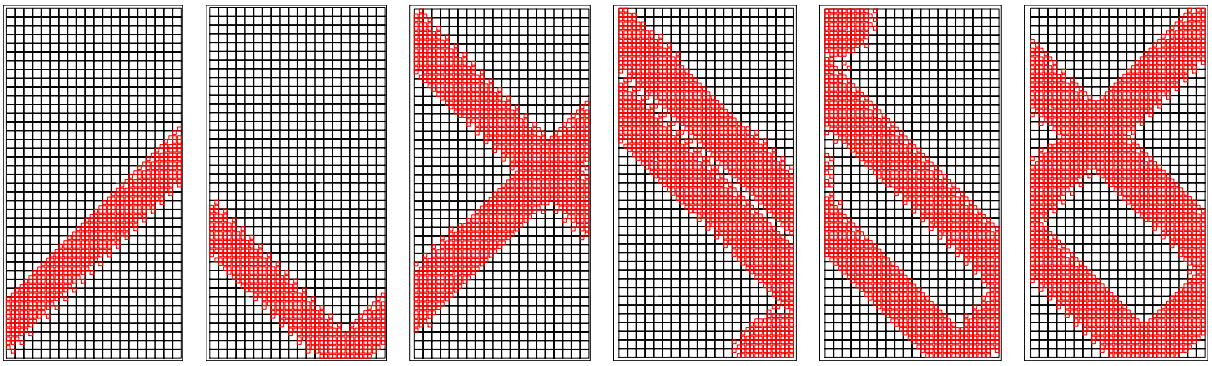

Figure 8. Example of localized solutions obtained after a random initialization, showing solutions with 1, 2 or 3 bands. The squares correspond to the integration points which are in the softening loading part; the other integration points are in the elastic part.

Figure 9 presents the global curves of the resulting force versus the axial shortening; they are clearly organized in several packages, each package being characterized by the number of deformation bands. This observation is similar to what has been seen in the one-dimensional case in [Chambon et al. 1998]. It is clear that the more numerous the bands are, the larger are the areas where plastic loading takes place, and, consequently, the closer the global curves are to the homogeneous case. We can observe that there is no difference between the case with bands crossing the specimen directly from a lateral surface to the opposite one and with band reflection, either on the top or on the bottom rigid plate.

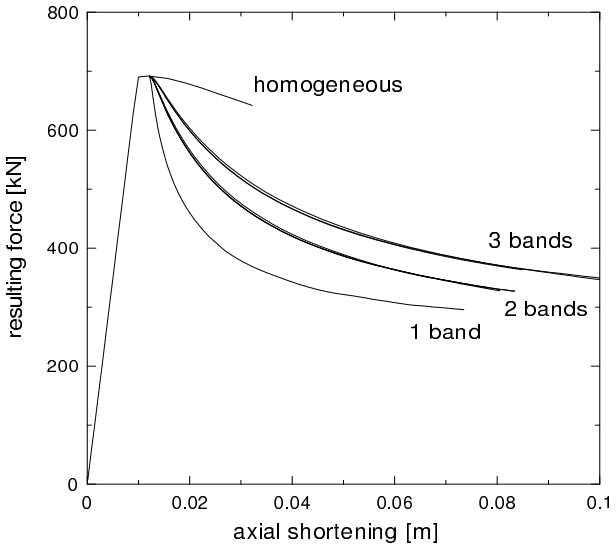

Figure 9. Comparison of the force versus axial shortening evolution of 10 simulations after a random initialization at a shortening of 0.012 m. Curves show that the responses depend on the number of bands. The higher the number of bands, the closer to the homogeneous response the curve is.

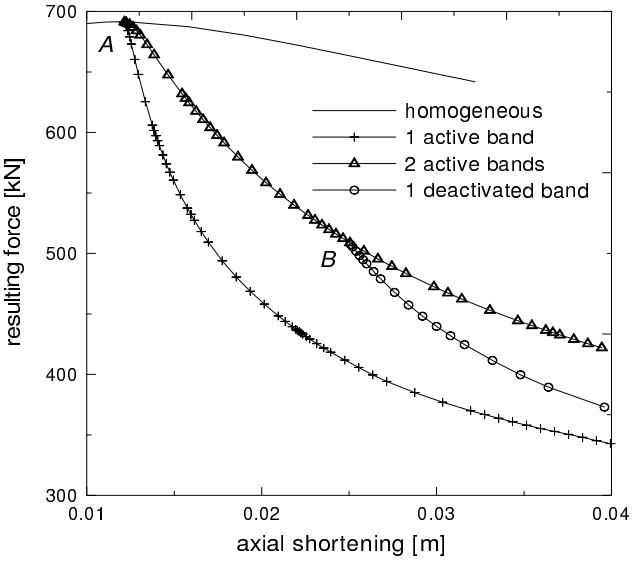

Figure 10. Comparison of the force versus axial shortening evolution in the postpeak regime of (converged) solutions with 1 active band, 2 active bands; and solution after the deactivation of one band. Step A corresponds to the random initialization, and step B corresponds to an *ad hoc* initialization in order to deactivate one band.

So, clearly these results show the nonuniqueness of solutions after the stress peak. The position and the number of bands are not prescribed by this boundary value problem, and we retrieve a variability of the responses similar to what is observed in experiments.

5.3. ***Numerical mode switching.*** From the initial homogeneous problem, after the onset of localization, several patterns of localization are possible for the numerical problem. The question addressed in this section is: is a given pattern stable, once activated? In fact, we will show that the pattern can evolve during the loading. If a solution has several bands which are active during the loading process, a solution for the next increment of loading is to keep all the bands active, but other solutions with fewer active bands are also possible. Since the areas outside the bands unload elastically, new bands cannot in fact appear, but it is possible that at a given time, some existing bands start to unload and become inactive.

To check this possibility, we use a method similar to the random initialization algorithm. The first guess used to start the Newton–Raphson iterative procedure is an *ad hoc* set of nodal values $[\Delta U^{t_n}_{\text{node}}]$ corresponding to a deactivation of some bands. An example of such a computation is shown for a two-band solution in Figure 10. A random initialization has been made for a specimen shortening of 0.012 m (step A), giving a two band solution, and the *ad hoc* initialization (step B) has been performed at a shortening of 0.025 m, to deactivate one of the bands. Then, the curve evolves from the two active band solutions to the one active band solution. The deformed meshes and the loading zones are shown in Figure 11 for an axial specimen shortening of 0.04 m. Figure 11, left, shows the result corresponding to a pattern of two active bands. The right hand side of the figure corresponds to a pattern where a band (the upper one) has been deactivated at step B. This figure shows clearly that the area corresponding to the deactivated band is still plastically deformed although it exhibits elastic unloading.

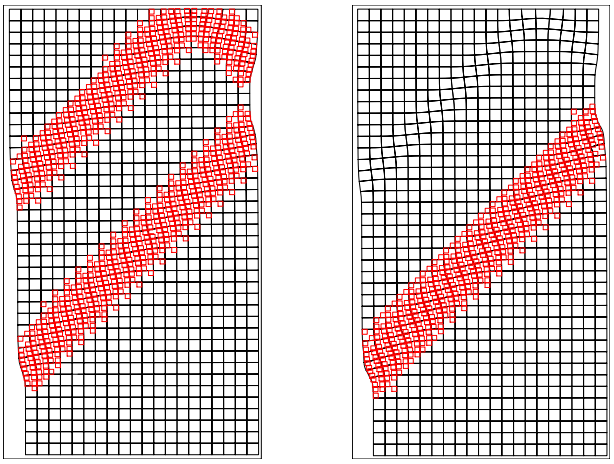

Figure 11. Pattern of active localization bands after the random initialization and (left) without deactivation of band, (right) after deactivation of the upper band. Deformed meshes correspond to the true deformation after a specimen shortening of 0.04 m, without displacement amplification.

6. Conclusion

To properly model localization patterns, the validation of the local second gradient theory has been extended. Localization analysis for this kind of model has been established. This theory is now mature and can be used in computation with some confidence. Similarly, the way of (partially) solving the bifurcation problem by means of different initializations of the Newton–Raphson iteration for a given time step has been extended to multiple bifurcations.

From a qualitative point of view, we are able to retrieve numerically the main features of observations made on experimental data. Especially, the great variability of the postpeak behavior of a sample is modeled realistically. These results have some consequences. First, the postpeak part of the curve cannot be interpreted as the result of a homogeneous response. Consequently, modeling the degradations of material needs enhanced models; moreover, the postpeak part of the curve can be used to get some material parameters only if the complete velocity field is known.

Clearly the results presented here have to be developed. Geomaterials are mainly polyphasic media, which implies the extension of the present model and methods to poromechanics. This has already been done; see [Collin et al. 2006] for details. Similarly, it is interesting to apply the methods presented to a classical constitutive equation less simple (elastic and sudden softening) than the one used here. This is work in progress [Bésuelle and Chambon 2006].

Finally a question arises. Is the loss of uniqueness observed and modeled for laboratory tests significant only for those tests for which homogeneity is required? In other words, can we find similar nonuniqueness problems for engineering situations? Answering such questions is not so easy, but some preliminary results [Al Holo 2005; Chambon and Al Holo 2006] indicate that for some problems, such as the borehole stability problem, the loss of uniqueness is important and may indicate poor reproducibility.

7. Acknowledgments

The authors thank R. Charlier (Liège) and D. Caillerie (Grenoble) for their helpful contributions.

References

[Al Holo 2005] S. Al Holo, *Etude numérique de la localisation à l'aide d'un modèle de second gradient : perte d'unicité et évolution de la zone localisée*, Ph.D. thesis, University of Grenoble, France, 2005.

[Bésuelle 2005] P. Bésuelle, "Implémentation d'un nouveau type d'élément fini dans le code Lagamine pour une classe de lois à longueur interne", Internal report, FNRS, Belgique, 2005. 1–17.

[Bésuelle and Chambon 2006] P. Bésuelle and R. Chambon, "Modelling the post-localization regime with local second gradient models: non uniqueness of solutions and non persistent shear bands", pp. 209–221 in *Modern trends in geomechanics*, edited by W. Wu and H. S. Yu, Springer, Berlin, 2006.

[Bésuelle and Rudnicki 2004] P. Bésuelle and J. W. Rudnicki, "Localization: shear bands and compaction bands", pp. 219–321 in *Mechanics of fluid-saturated rocks*, edited by Y. Guéguen and M. Boutéca, International geophysics series **89**, Elsevier, 2004.

[Borja 2002] R. I. Borja, "Bifurcation of elastoplastic solids to shear band mode at finite strain", *Mech. Engng.* **191** (2002), 5287–5314.

[de Borst 1986] R. de Borst, *Non linear analysis of frictional materials*, Ph.D. thesis, University of Delft, Netherlands, 1986.

[Challamel and Hijaj 2005] N. Challamel and M. Hijaj, "Non local behavior of plastic softening beams", *Acta Mechanica* **178** (2005), 125–146.

[Chambon and Al Holo 2006] R. Chambon and S. Al Holo, "The borehole stability problem revisited", 2006. in preparation.

[Chambon and Moullet 2004] R. Chambon and J. C. Moullet, "Uniqueness studies in boundary value problems involving some second gradient models", *Comput. Meth. Appl. Mech. Engng.* **193** (2004), 2771–2796.

[Chambon et al. 1998] R. Chambon, D. Caillerie, and N. El Hassan, "One dimensional localisation studied with a second grade model", *Eur. J. Mech. A/Solids* **17** (1998), 637–656.

[Chambon et al. 2000] R. Chambon, S. Crochepeyre, and J. Desrues, "Localization criteria for non-linear constitutive equations of geomaterials", *Mech. Cohesive-Frictional Mater.* **5** (2000), 61–82.

[Chambon et al. 2001a] R. Chambon, D. Caillerie, and T. Matsushima, "Plastic continuum with microstructure, local second gradient theories for geomaterials: localization studies", *Int. J. Solids Struct.* **38**:46-47 (2001a), 8503–8527.

[Chambon et al. 2001b] R. Chambon, S. Crochepeyre, and R. Charlier, "An algorithm and a method to search bifurcation point in non linear problems", *Int. J. Numer. Meth. Engng.* **51** (2001b), 315–332.

[Chambon et al. 2004] R. Chambon, D. Caillerie, and C. Tamagnini, "A finite deformation second gradient theory of plasticity", *Comput. Meth. Appl. Mech. Engng.* **193** (2004), 2797–2826.

[Charlier 1987] R. Charlier, *Approche unifiée de quelques problèmes non linéaires de mécanique des milieux continus par la méthode des éléments finis*, Ph.D. thesis, University of Liège, Belgium, 1987.

[Collin et al. 2006] F. Collin, R. Chambon, and R. Charlier, "A finite element method for poro mechanical modelling of geotechnical problems using local second gradient models", *Int. J. Numer. Meth. Engng.* **193** (2006), 2771–2796.

[Cosserat and Cosserat 1909] E. Cosserat and F. Cosserat, *Théorie des corps déformables*, Hermann, Paris, 1909.

[Desrues 1984] J. Desrues, *La localisation de la déformation dans les matériaux granulaires*, Ph.D. thesis, University of Grenoble, France, 1984.

[Desrues and Hammad 1985] J. Desrues and W. Hammad, "Shear banding dependency on mean stress level in sand", pp. 57–68 in *Proc. 2nd Int. Workshop on Localisation and Bifurcation*, edited by E. Dembicki et al., Techn. Univ. Gdansk, Gdansk, 1985.

[Desrues and Viggiani 2004] J. Desrues and G. Viggiani, "Strain localization in sand: an overview of the experimental results obtained in Grenoble using stereophotogrammetry", *Int. J. Numer. Anal. Meth. Geomech.* **28** (2004), 279–321.

[El Hassan 1997] N. El Hassan, *Modélisation théorique et numérique de la localisation de la déformation dans les géomatériaux*, Ph.D. thesis, University of Grenoble, France, 1997.

[Fleck and Hutchinson 1997] N. A. Fleck and J. W. Hutchinson, "Strain gradient plasticity", *Advances Appl. Mech., Academic Press* **33** (1997), 295–361.

[Germain 1973] P. Germain, "La méthode des puissances virtuelles en mécanique des milieux continus, première partie : théorie du second gradient", *J. Méc.* **12**:2 (1973), 235–274.

[Hill 1958] R. Hill, "A general theory of uniqueness and stability in elastic-plastic solids", *J. Mech. Phys. Solids* **6** (1958), 236–249.

[Huang et al. 2005] W. Huang, M. Hijaj, and S. C. Sloan, "Bifurcation analysis for shear localization in non-polar and micro-polar hypoplastic continua", *J. Engng. Math.* **52** (2005), 167–184.

[Ikeda and Murota 2002] K. Ikeda and K. Murota, *Imperfect bifurcation in structures and materials*, Springer, Berlin, 2002.

[Ikeda et al. 1997] K. Ikeda, K. Murota, Y. Yamakawa, and E. Yanagisawa, "Modes switching and recursive bifurcation in granular materials", *J. Mech. Phys. Solids* **45** (1997), 1929–1953.

[Ikeda et al. 2003] K. Ikeda, Y. Yamakawa, and S. Tsutumi, "Simulation and interpretation of diffuse mode bifurcation of elastoplastic solids", *J. Mech. Phys. Solids* **51** (2003), 1649–1673.

[Iordache and Willam 1998] M. M. Iordache and K. Willam, "Localized failure analysis in elastoplastic Cosserat continua", *Comput. Meth. Appl. Mech. Engng.* **193** (1998), 559–586.

[Matsushima et al. 2002] T. Matsushima, R. Chambon, and D. Caillerie, "Large strain finite element analysis of a local second gradient model: application to localization", *J. Numer. Meth. Engng.* **54** (2002), 499–521.

[Mindlin 1964] R. D. Mindlin, "Micro-structure in linear elasticity", *Arch. Rat. Mech. Anal.* **4** (1964), 50–78.

[Nübel and Huang 2004] K. Nübel and W. Huang, "A study of localized deformation pattern in granular media", *Comput. Meth. Appl. Mech. Engng.* **193** (2004), 2719–2743.

[Pijaudier-Cabot and Bažant 1987] G. Pijaudier-Cabot and Z. Bažant, "Nonlocal damage theory", *J. Engng. Mech.* **113** (1987), 1512–1533.

[Rice 1976] J. R. Rice, "The localization of plastic deformation", pp. 207–220 in *14th Int. Cong. Theor. Appl. Mech.*, edited by W. T. Koiter, Theoretical and Applied Mechanics (North-Holland Pub. Comp., Delft, 1976.

[Rudnicki and Rice 1975] J. W. Rudnicki and J. R. Rice, "Conditions for the localization of deformation in pressure-sensitive dilatant materials", *J. Mech. Phys. Solids* **23** (1975), 371–394.

[Steinmann et al. 1997] P. Steinmann, R. Larsson, and K. Runesson, "On the localization properties of multiplicative hyper-elasto-plastic continua with strong discontinuities", *Int. J. Solids Struct.* **34** (1997), 969–990.

[Tamagnini et al. 2001b] C. Tamagnini, R. Chambon, and D. Caillerie, "A second gradient elastoplastic cohesive frictional model for geomaterials", *C.R.A.S-Série II b.* **329** (2001b), 735–739.

[Toupin 1962] R. A. Toupin, "Elastic materials with couple-stresses", *Arch. Rat. Mech. Anal.* **11** (1962), 385–414.

[Viggiani et al. 2001] G. Viggiani, M. Küntz, and J. Desrues, *Continuous and discontinuous modelling of cohesive-frictional materials*, Chapter An experimental investigation of the relationships between grain size distribution and shear banding in sand, pp. 111–127, Springer, Berlin, 2001.

Received December 11, 2005.

PIERRE BÉSUELLE: Pierre.Besuelle@hmg.inpg.fr
Laboratoire 3S, Grenoble, Université Joseph Fourier, Institut National Polytechnique, C.N.R.S. U.M.R. 5521, B.P. 53X, 38041 Grenoble Cedex 9, France

RENÉ CHAMBON: Rene.Chambon@hmg.inpg.fr
Laboratoire 3S, Grenoble, Université Joseph Fourier, Institut National Polytechnique, C.N.R.S. U.M.R. 5521, B.P. 53X, 38041 Grenoble Cedex 9, France

FRÉDÉRIC COLLIN: F.Collin@ulg.ac.be
Geomac, FNRS-ULG, Liège, Belgium